

Second MAYA Catalog of Binary Black Hole Numerical Relativity Waveforms

Deborah Ferguson¹, Evelyn Allsup¹, Surendra Anne¹, Galina Bouyer¹, Miguel Gracia-Linares¹, Hector Iglesias¹, Aasim Jan¹, Pablo Laguna¹, Jacob Lange¹, Erick Martinez¹, Filippo Meoni¹, Ryan Nowicki¹, Deirdre Shoemaker¹, Blake Steadham¹, Max L. Trostel¹, Bing-Jyun Tsao¹, and Finny Valorz¹

¹*Center for Gravitational Physics and Department of Physics,
The University of Texas at Austin, Austin, TX 78712*

Numerical relativity waveforms are a critical resource in the quest to deepen our understanding of the dynamics of, and gravitational waves emitted from, merging binary systems. We present 181 new numerical relativity simulations as the second MAYA catalog of binary black hole waveforms (a sequel to the Georgia Tech waveform catalog). Most importantly, these include 55 high mass ratio ($q \geq 4$), 48 precessing, and 92 eccentric ($e > 0.01$) simulations, including 7 simulations which are both eccentric and precessing. With these significant additions, this new catalog fills in considerable gaps in existing public numerical relativity waveform catalogs. The waveforms presented in this catalog are shown to be convergent and are consistent with current gravitational wave models. They are available to the public at <https://cgp.ph.utexas.edu/waveform>.

I. INTRODUCTION

Gravitational wave observations have become increasingly frequent, with the LIGO Scientific, Virgo and KAGRA Collaborations (LVK) reporting 90 detections through the end of their third observing run, including 83-85 likely binary black holes (BBHs) [1–4], and more are expected in the fourth observing run. The BBH systems observed by the LVK span a large range of parameters, including mass ratios from equal mass to the possible 9:1 mass ratio of GW190814 [5]. While most of the events are consistent with nonspinning black holes (BHs), some show evidence of strong precession [1], and some events even show signs of eccentricity [6, 7]. As we prepare for next-generation gravitational-wave detectors such as the Laser Interferometer Space Antenna (LISA) [8–10], the Einstein Telescope (ET) [11, 12], and Cosmic Explorer (CE) [13], we anticipate a significant increase in the volume of signals as well as a more diverse parameter space. Understanding the properties of the systems these signals come from and their underlying populations [14] and using the signals to test General Relativity (GR) [15] relies upon having accurate predictions of the anticipated signals.

Due to the complex nature of Einstein’s theory of GR, analytic solutions don’t exist for the full two body problem of merging compact objects. A number of techniques have been developed to solve for the dynamics and radiation of such systems, and the most appropriate technique depends upon the parameters of the binary system in question. When the objects are far apart, post-Newtonian (PN) approximations can be used with high accuracy and confidence [16–22]. For systems where the masses of the black holes are highly unequal, small mass ratio approximations allow for efficient simulations [23–25]. Great progress has also been made towards using small mass ratio approximations for the inspiral of near equal mass ratio systems [26–30].

In the highly nonlinear regime of the merger of comparably massed compact objects, numerical relativity (NR)

is the most accurate approach. NR computationally solves Einstein’s equations by expressing them in a 3+1 formalism and separating the constraint and evolution equations in order to create an initial value problem that can be evolved on a computer [31–33]. For the case of BBHs in vacuum, there is no missing physics within the simulations, as long as GR is correct, and the only limitations are computational in nature. A NR simulation will solve Einstein’s equations for a single binary system described by the masses and spin vectors of the two component BHs. For BBHs in vacuum, the results of the simulation can be scaled by the total mass, so we set the total ADM mass of the system to 1, and the masses can then simply be described by the mass ratio, $q = m_1/m_2 \geq 1$. By creating template banks of NR simulations, NR waveforms have been used directly in gravitational wave (GW) detection and parameter estimation [6, 34–36].

These simulations are placed discretely throughout the parameter space and are time consuming and computationally expensive. Therefore, while NR waveforms can be used directly as template banks for GW analysis, for many analyses, analytic or semi-analytic models are created, using information from NR for calibration [37–46]. However, creating reliable models and template banks relies upon NR waveforms being sufficiently accurate and densely covering the complete parameter space [47, 48].

There are several NR codes and public waveform catalogs created by the NR community. The SXS collaboration has a public waveform catalog generated using their SpEC code [49, 50] and have been developing their next-generation code, SpECTRE [51]. There are several waveform catalogs generated with codes derived from an open source software used by many NR groups [52], the *Einstein Toolkit* [53–57]. The waveforms in the catalog presented in this paper are also generated with a code derived from the *Einstein Toolkit*, called *Maya*.

We previously released the Georgia Tech waveform catalog [53] using our *Maya* code including 452 waveforms covering the spinning parameter space up to $q = 8$ and including nonspinning waveforms up to $q = 15$.

These waveforms have been used to study exceptional LVK events [34], the detectability of intermediate-mass BHs [58–60], as well as post-merger chirps [61], to highlight a few recent studies. They have also been used to study the different stages of the merger, including finding a relationship between the frequency at merger and the spin of the remnant BH [62, 63]. Using the Georgia Tech catalog, it was also found that the BH recoil can be measured from GW observations [64], a method which has been applied to real events [65]. This catalog has since been rebranded to the MAYA Catalog.

This paper introduces the second MAYA Catalog, expanding beyond the parameter space coverage of the first catalog and introducing a new format. This format can be read using the `mayawaves` python library [66, 67], which is described further in Section II B. The new catalog includes a suite of eccentric simulations as well as improved coverage of the high mass ratio parameter space and the precessing parameter space. In Section II, we describe the `Maya` code used to create this catalog as well as the `mayawaves` python library. We then dive into the description of the new catalog in Section III. Section IV compares our simulations to other NR waveforms and waveform models, including an eccentric model, and Section V compares the models for the remnant BH parameters to the results obtained from our catalog. Finally, in Section VI, we include a discussion of the impact of center-of-mass (COM) drift corrections.

II. CODEBASE

In this section, we’ll describe the code used to perform these NR simulations (`Maya`) as well as the python library used to interact with and analyze the simulations (`mayawaves`).

A. Maya Code

This catalog was constructed from simulations performed using the `Maya` code, a fork of the *Einstein Toolkit* using additional and modified thorns. The *Einstein Toolkit* is a finite-differencing code based upon the *Cactus* infrastructure using *Carpets* for box-in-box mesh refinement [68]. `Maya` uses the BSSN formulation [31] to separate Einstein’s equations into constraint equations to solve for the initial data and evolution equations to evolve the spacetime. The initial data consists of the extrinsic curvature and the spatial metric and is constructed using the TwoPunctures method [69]. The extrinsic curvature takes the Bowen-York form [70], and the initial spacial metric is conformally flat. To set the initial momenta for quasi-circular simulations, we use the PN equations described in [71]. We use the moving puncture gauge condition [72, 73] and use the `Kranc` scripts to generate the thorns for the spacetime evolution [74].

The Weyl Scalar is computed throughout the computational domain (x,y,z) , but to interpret it as gravitational radiation, it is extracted at several radii and extrapolated to spatial infinity. The waves are then decomposed and stored using the spin-weighted spherical harmonics as a basis:

$$RM\Psi_4(t; \Theta, \Phi) = \sum_{\ell,m} \Psi_{4;\ell,m}(t) {}_{-2}Y_{\ell,m}(\Theta, \Phi), \quad (1)$$

where R is the extraction radius, M is the total mass of the binary, and Θ and Φ specify the location on the sphere centered at the COM of the binary. We provide the gravitational wave data at several extraction radii and `mayawaves` can be used to extrapolate the data to infinity using the method described in [45, 75]. `mayawaves` also allows you to compute the strain, $h(t)$, which is related to Ψ_4 by the following:

$$\Psi_4(t) = \ddot{h}(t)_+ - i\dot{h}(t)_\times. \quad (2)$$

In our previous catalog paper, we showed that the `Maya` code is convergent [53]. Since this catalog introduces eccentric simulations, we include a convergence test for a simulation that is representative of the suite of included eccentric simulations. We consider a nonspinning system with $q = 2$ and eccentricity, $e = 0.05$ for three different resolutions, $1/\Delta_{low} = 141.18$, $1/\Delta_{med} = 211.76$, and $1/\Delta_{high} = 282.35$. Figure 1a shows the residuals scaled by the factor a , defined as:

$$a = \frac{\Delta_{high}^\alpha - \Delta_{med}^\alpha}{\Delta_{med}^\alpha - \Delta_{low}^\alpha}, \quad (3)$$

where α is the convergence rate which proves to be 2.36 for this simulation. We use 6-th order spacial finite differencing and 4th order Runge-Kutta for time evolution. Given the complex mesh refinement and the interpolation necessary to extract Ψ_4 on spheres, this convergence rate is as expected.

We use the results from our convergence test to estimate the errors in our highest resolution waveform. Figure 1b shows the estimated error in our highest resolution waveform for this system. Based on the method presented in [47], this will be indistinguishable from an “infinite” resolution face-on signal up to a signal-to-noise ratio (SNR) of $\rho = 242$.

B. mayawaves Python Library

The simulations in this catalog are provided in two formats. The more comprehensive format consists of an h5 file for each simulation that contains information relating to the compact objects as well as the radiation they emit. This h5 file should be read using the `mayawaves` python library [66, 67]. This library provides easy and efficient use of the MAYA catalog and can also be used to analyze any *Einstein Toolkit* simulation. Storing the

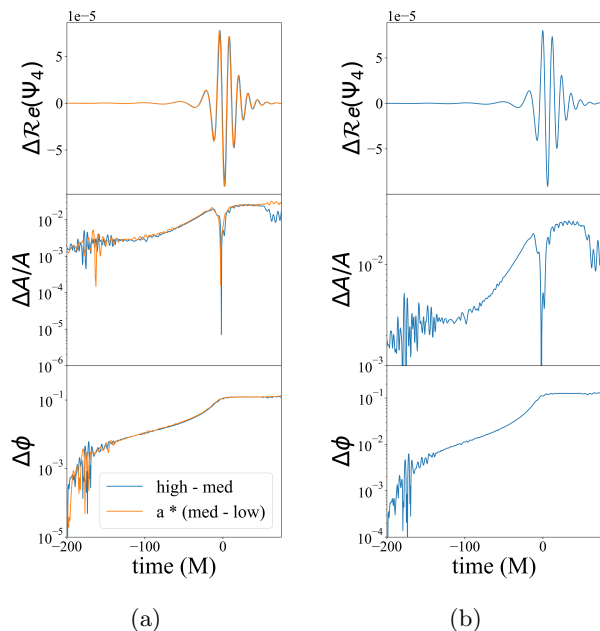


FIG. 1: Error analysis for an eccentric simulation. (a) shows the convergence with resolution by showing the residuals using the high and medium resolutions (blue) and the medium and low resolutions (orange). The residual using the medium and low resolutions is scaled according to the convergence factor using Eq. 3. (b) shows the estimated error in the highest resolution waveform.

simulations in this format enables us to provide more raw data pertaining to radiated quantities as well as the evolution of the compact objects themselves. The user need only download the desired waveform from our catalog, import `mayawaves` in their python file, and create a `Coalescence` object by passing in the simulation’s path to the constructor. They can then access all information regarding the simulation through the `Coalescence` object. The `mayawaves` library can be installed via pip or from source at <https://github.com/MayaWaves/mayawaves>. Documentation and tutorials can be found at <https://mayawaves.github.io/mayawaves>. Refer to [66] for more information on this library.

III. CATALOG DESCRIPTION

The MAYA catalog of NR waveforms is accessible at <https://cgp.ph.utexas.edu/waveform>. At that location, you will see a table with the metadata describing each simulation in the catalog. From that table, you can download each of the simulations. They are stored in an h5 format that is designed to be read using the `mayawaves` python library. Any simulations that contain all the necessary data are also provided in the format detailed in [76] for use with PyCBC [77, 78].

This catalog introduces 181 new simulations that expand our coverage of the BBH parameter space, for a total of 635 simulations. The catalog website has also been updated to include the original catalog [53] in the new `mayawaves` compatible format. Figure 2 shows the coverage of the previous catalog and this catalog, highlighting the many more eccentric simulations, precessing simulations, and high mass ratio simulations introduced by this catalog. Figure 3 shows the spin coverage of the combined catalogs. Figure 4 shows the distribution of the number of inspiral GW cycles after junk radiation for each simulation in the original and new catalogs. Simulations in the new catalog have a median of ~ 16.5 GW cycles and the overall catalog has a median of ~ 11 GW cycles.

This catalog is an amalgamation of several suites of simulations performed for various studies. This includes a suite of 80 non-precessing, eccentric simulations with mass ratios up to $q = 4$. It includes 38 simulations for a study of secondary spin for mass ratios up to $q = 15$. We also include 9 simulations performed for LVK followup studies. Finally we have 31 simulations placed to optimally fill in gaps in our parameter space using the network and method described in [79]. Each of these suites is described in more detail below. The remaining 23 simulations are an assortment of simulations performed over the last few years.

A. Eccentric

As orbits evolve, eccentricity is quickly radiated away [80]; therefore, for most scenarios, the eccentricity is expected to be minimal by the time a stellar mass BBH system reaches current ground-based GW detectors’ frequency bands. As a consequence, most NR simulations and GW models have focused on quasicircular binary systems. However, there are astrophysical situations that can lead to non-zero eccentricity in binaries observed by ground-based detectors [7, 81–84]. Some future GW detectors such as LISA, will observe many binaries earlier in their inspiral and are expected to see some eccentricity remaining within the signals. In order to be prepared to detect and study these signals, we will need eccentric NR simulations and eccentric GW models. In fact, some LVK events have already shown potential evidence for eccentricity, increasing the urgency with which we need to explore this parameter space [6, 7]. As part of this catalog, we have included 92 new eccentric simulations.

80 of these simulations were part of a systematic suite designed to explore the eccentric space. They have mass ratios of $1 \leq q \leq 4$ by steps of 1, and for each q , we have $a_1 = a_2 = \{0, 0.4\}$ aligned with the orbital angular momentum. For each of the above cases, we performed simulations with eccentricity, $0.01 \leq e \leq 0.1$ by steps of 0.01. These simulations have catalog ids of MAYA0913-MAYA0931, MAYA0938-MAYA0947, MAYA0949-MAYA0958, MAYA0960-MAYA0969,

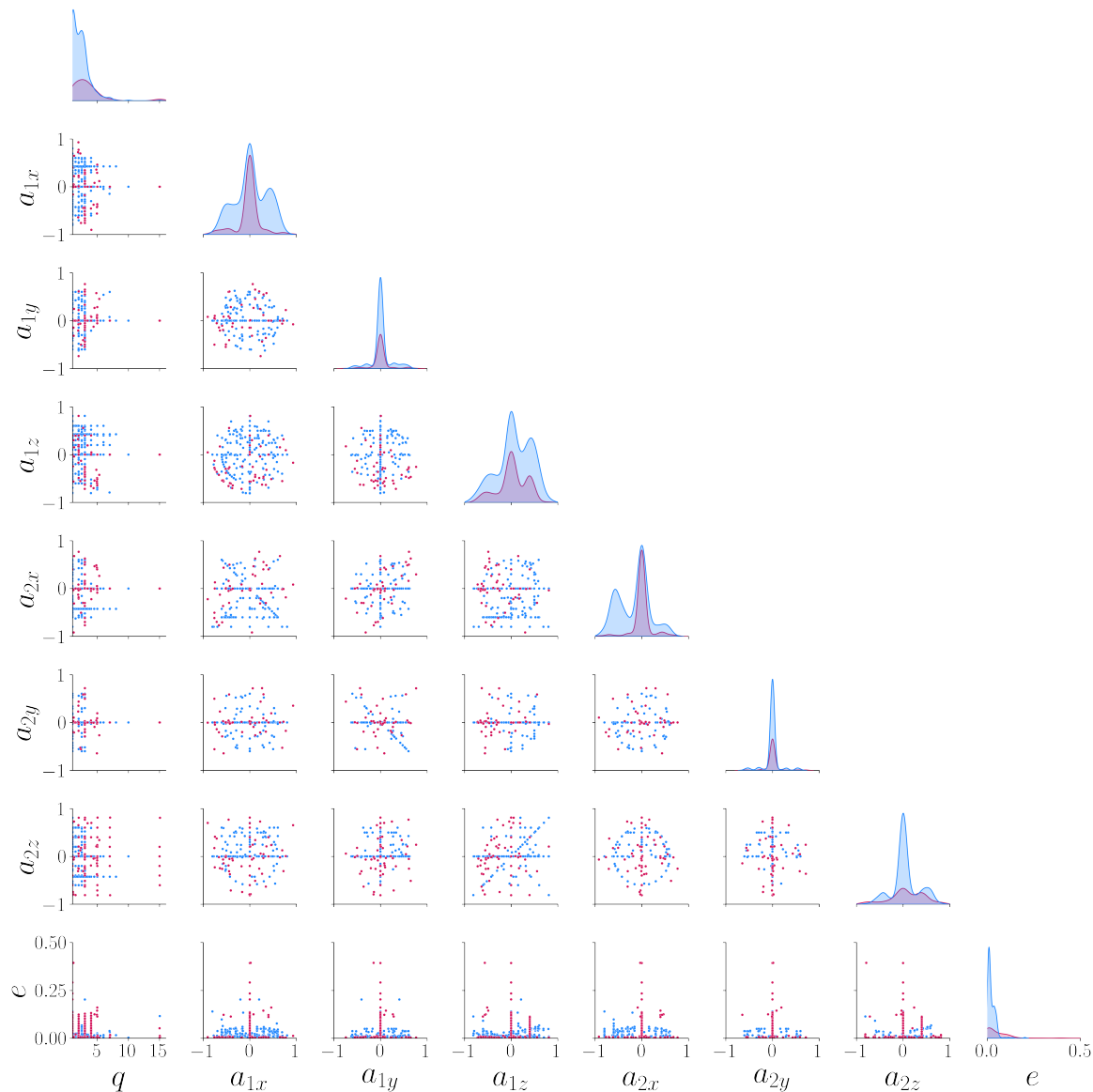


FIG. 2: Coverage of the parameter space for the original catalog (blue) and the new catalog (pink).

MAYA0971-MAYA0980, MAYA0982-MAYA1001, and MAYA1041. For each q , a_1 , a_2 combination, the catalog also includes a quasicircular simulation.

Since eccentricity is a Newtonian concept, there is no unambiguous definition of eccentricity within GR. The `mayawaves` library currently uses the orbital frequency definition described in [85]. This definition has proved to be robust and consistent with other definitions of eccentricity. For setting up the eccentric simulations, we use the method described in [6], applying a Newtonian derived correction to the quasicircular momentum. Since this definition is based on Newtonian assumptions, the resulting eccentricities are not exactly the same as the target eccentricities. As we are aiming to generally fill out the eccentric space and do not need precise values of

$e = 0.01, 0.02, \dots$, we do not apply iterative corrections to target the exact eccentricity values.

We also include 5 additional simulations with $q = 1$ and eccentricities up to $e = 0.6$. These have catalog ids of MAYA0932-MAYA0936. Additionally, we have 7 simulations with both eccentricity and precession, with ids MAYA1043-MAYA1049. These are particularly useful since there are currently no eccentric, precessing waveform models.

B. Secondary Spin

We performed a suite of simulations spanning mass ratios of $q = 1, 3, 5, 7, 15$ with varying spins, including

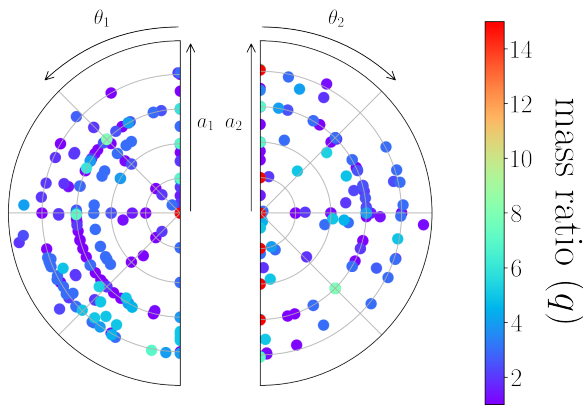


FIG. 3: Coverage of the spin parameter space. The left semicircle denotes the spin for the primary black hole, with radius showing dimensionless spin magnitude (a_1) and the angle from the vertical showing the angle between the spin and the orbital angular momentum (θ_1). The same applies for the secondary black hole (a_2 and θ_2), shown on the right semicircle. The color denotes the mass ratio.

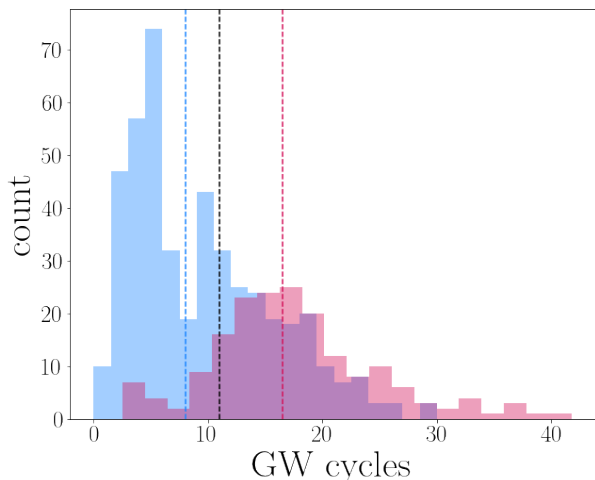


FIG. 4: Distribution of the number of inspiral GW cycles for the simulations in the original catalog (blue) and the new catalog (pink). The vertical lines denote the medians.

9 simulations with $q = 15$. The primary BH is non-spinning and the secondary BH has an aligned spin of $-0.8 \leq a_2 \leq 0.8$ by steps of 0.2. Current public NR catalogs have minimal coverage of the parameter space with $q > 4$, especially with secondary spin. These simulations help fill that gap. This suite also enables us to study the impact of the secondary spin as a function of mass ratio. The simulations with $q = 1, 3, 5, 7$ begin with a separation of $D = 11M$ and the $q = 15$ simulations begin at $D = 10M$. This suite includes simulations with

ids MAYA1002-MAYA1039.

C. LVK Followup

Some of the detections made by the LVK have required additional NR followup. This is particularly useful for events that push to the edges of the regions where models are sufficiently trained or in situations where different models yield inconsistent posteriors for the parameters of the binary. We performed 7 simulations (MAYA1050-MAYA1056) as followup for GW190521, an event that has been the focus of a lot of different studies due to its limited number of cycles [6, 7, 86–88]. By using RIFT to perform parameter estimation on GW190521 with NR simulations, these points in parameter space were identified as locations with both high likelihood and high uncertainty in the fit [34]. Performing simulations at these points and then repeating the RIFT analysis with the new waveforms included is expected to improve the accuracy of and confidence in the estimated parameters for GW190521. Also for GW190521, we performed a simulation at the point of maximum likelihood for the purpose of visualizations for the announcement of the first intermediate-mass BH observation. We also performed one simulation (MAYA0912) as followup for GW170608.

D. Optimized Template Placement

Many of our simulations are performed for specific studies and thus have very specific initial parameters. However, in order to prepare for future LVK runs and next-generation detectors, we also want to fill out our catalog in an efficient and strategic way. To accomplish this, we use the neural network presented in [79] and the method it describes to identify optimal parameters. This method makes use of a neural network trained to predict the match between any two quasi-circular binary systems given their initial parameters. Using this network, we search for the minimal match between potential simulations and those already existing in the catalog. Given the non-smooth nature of the space, we use basin hopping to identify global minima.

This tool has enabled us to identify and perform simulations in a way that maximally fills in gaps in our coverage. We have just begun to use this tool and have performed 31 simulations suggested by it, with ids MAYA1057-MAYA1087. These simulations have mass ratios up to $q = 5$ and precessing spins up to magnitudes of 0.8. Current catalogs have dense coverage in low mass-ratio spaces, but have minimal coverage above $q = 4$. In general, the precessing space is also much less densely covered than the aligned spin space. These 31 simulations make significant improvements to the coverage of the moderate to high mass-ratio, precessing parameter space. This tool will play a large role in the generation of waveforms for our future catalogs.

IV. WAVEFORM COMPARISONS

Within the NR community, there are several different methods and techniques for solving Einstein’s equations directly. While each method has its benefits and drawbacks, all NR waveforms are considered to be the gold standard for studying the merger of comparable-mass BBH systems. To ensure accuracy and consistency in analyses that use NR waveforms of each technique, it is important to perform cross-code comparisons. Several of these have been done over the past couple decades, and the methods used by the *Einstein Toolkit* and the Simulating eXtreme Spacetimes (SXS) Collaboration have proven to be reliable [89–91]. Here, we provide a comparison between this catalog and comparable waveforms available in the SXS catalog.

Similarly, there are many analytic and semi-analytic models for computing GWs. These models have the benefit of being faster than NR allowing for continuous sampling of the parameter space. However, given that these models are trained or calibrated to NR waveforms, they are generally not considered to be as accurate as NR waveforms. In this section we will also perform a comparison between this catalog and waveforms generated using such models.

For each of these comparisons, we compute the mismatch on a flat noise curve, defined as:

$$\mathcal{MM} = 1 - \max_{t, \phi} \mathcal{O}[h_1, h_2] \equiv 1 - \max_{t, \phi} \frac{\langle h_1 | h_2 \rangle}{\sqrt{\langle h_1 | h_1 \rangle \langle h_2 | h_2 \rangle}}, \quad (4)$$

where

$$\langle h_1 | h_2 \rangle = 2 \int_{f_0}^{\infty} \frac{h_1^* h_2 + h_1 h_2^*}{S_n} df, \quad (5)$$

with S_n being a flat PSD, and $*$ denoting the complex conjugate. Mismatches are very sensitive to systematic effects such as the amount of tapering and the starting frequency, and we find that these effects can change the mismatches by up to $\sim 10^{-3}$. For consistency and to reduce Gibbs oscillations, we consider only waveforms with more than 10 inspiral cycles and taper 6 of them. We compute all mismatches using a total mass of $M_{tot} = 100M_{\odot}$ and a starting frequency of 30 Hz.

For the SXS comparison, we consider all equivalent non-precessing systems that exist in our catalog and in the SXS LVK catalog. Figure 5a shows the mismatch as a function of inclination, using all available modes and a flat noise curve. The grey lines show each individual system and the black line shows the median. Figure 5b shows the distribution of mismatches (including all 20 inclinations) with a median mismatch of 10^{-3} .

We also compare our waveforms to the current state-of-the-art waveform models. For the quasicircular case, we compare to IMRPhenomXPHM [46] for both precessing and non-precessing systems, and for the eccentric case, we compare to TEOBResumS-DALI [92–95]. Figure 6a

shows the mismatch between the quasicircular NR waveforms and the IMRPhenomXPHM waveforms as a function of inclination, including all available modes on a flat noise curve. Each of the precessing systems appears as a faint orange line with the vibrant orange line showing the median value for all precessing simulations. All non-precessing simulations appear as faint blue lines with the vibrant blue line showing the median value for all non-precessing simulations. The black line shows the median mismatch of all quasicircular simulations. Figure 6b shows the distribution of the mismatches for precessing (blue) and aligned (orange) systems including 20 uniformly distributed inclinations. For non-precessing systems, the median mismatch is $\sim 10^{-3}$, and for the precessing systems, the median mismatch is $\sim 2 \times 10^{-2}$.

For the eccentric case, we use TEOBResumS-DALI as the waveform model and consider only aligned spin systems. We optimize over the initial eccentricity and frequency of the model waveforms to obtain the best mismatch, since the model’s eccentricity parameter is not physically meaningful. Figure 7 shows the mismatches between TEOBResumS-DALI waveforms and 20 of our waveforms which fall within the validity range of the model ($e \leq 0.2$, $q \leq 3$, and $a_1, a_2 \leq 0.7$). The median mismatch over all systems and inclinations is $\sim 5 \times 10^{-3}$.

V. FINAL MASS, SPIN, AND KICK

In this section, we compare the properties of the remnant BH computed from NR simulations to those predicted using NRSur7dq4Remnant [37]. We use the SurfinBH python library [96, 97] to interact with NRSur7dq4Remnant and compute the predicted remnant properties. We provide the masses and spins of the initial BHs at a time $100M$ before merger, rotated into the same frame used by NRSur7dq4Remnant. We only consider systems which fall within the range of validity for NRSur7dq4Remnant ($q \leq 4$ and dimensionless spin parameters $a_1, a_2 \leq 0.8$). The masses and spins of the initial and remnant BHs are computed from the BH apparent horizons, and the magnitude of the kick velocity is computed from the linear momentum radiated by the GWs.

Figure 8 shows the remnant properties obtained from NR simulations compared to the remnant properties obtained from NRSur7dq4Remnant. For each of the remnant properties, the non-precessing systems have much lower errors than the precessing systems. However, for remnant spin, all residuals fall within 0.0125, and for remnant mass, all residuals fall within 0.0012. The recoil velocity is more challenging since it is very sensitive to spin angles. The system with the largest residual has an error of 29%.

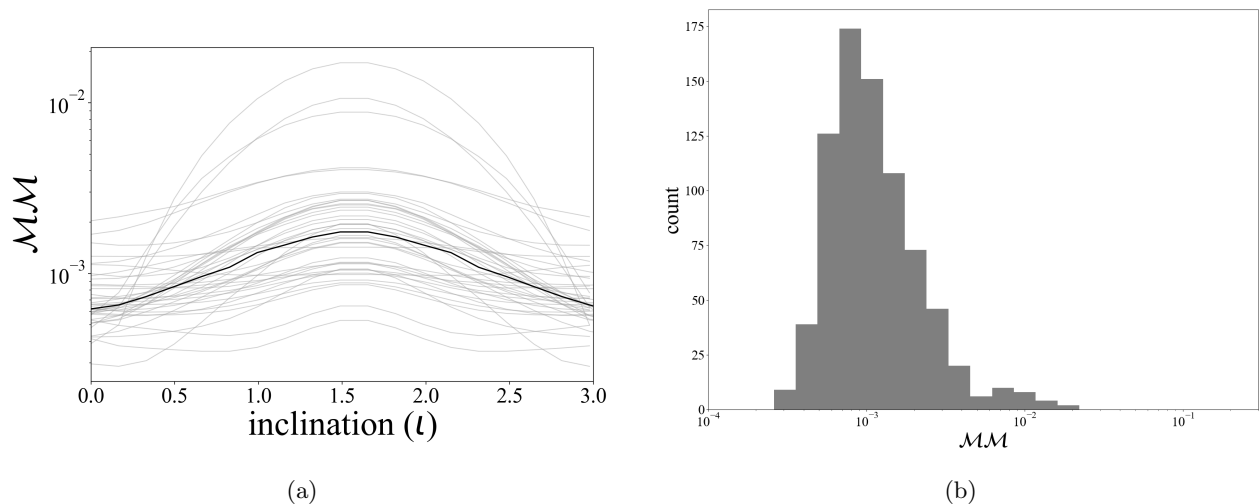


FIG. 5: Mismatches between quasicircular, non-precessing MAYA waveforms and SXS waveforms using a flat noise curve over 20 different values of inclination. a) Mismatches as a function of inclination. The black line is the median for all systems. The faint lines show all of the individual systems. b) Distribution of mismatches.

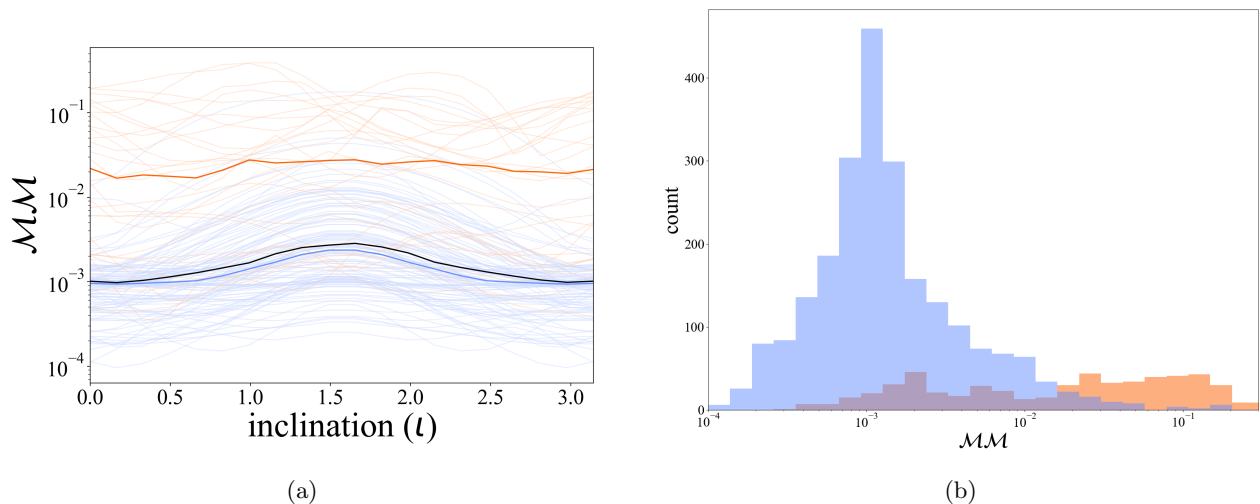


FIG. 6: Mismatches between quasicircular MAYA waveforms and IMRPhenomXPHM waveforms using a flat noise curve over 20 different values of inclination. Orange denotes precessing systems and blue denotes non-precessing systems. a) Mismatches as a function of inclination. The bright orange and blue lines show the median of the precessing and non-precessing systems respectively. The black line is the median for all included waveforms. The faint lines show all of the individual systems. b) Distribution of mismatches.

VI. CENTER OF MASS DRIFT CORRECTIONS

During the NR simulation of the inspiral of BBH systems, the center of mass experiences a wobble and a drift. These are caused by a combination of physical effects due to the asymmetrical emission of GWs and numerical error. Since the GWs are decomposed with the spherical harmonics centered on the initial COM, this can cause mode mixing. In recent years there has been much discussion of the impact that these COM drifts can cause to the waveform modes. We include here a brief analysis

of the impact of correcting for such drifts.

Using the Scri python package [98–101], we apply corrections for a translation and boost in the COM, computed using equations 6 and 7 of [102]. We then perform a mismatch analysis comparing the COM corrected waveforms and the uncorrected waveforms for the overall strain and for individual modes. Figure 9 shows the mismatches between raw and COM corrected strains. In Figure 9a, we see the mismatch with all modes combined as a function of inclination. The median mismatch is fairly constant for all inclinations, with a value of $\sim 4 \times 10^{-5}$. In Figure 9b, we see the mismatch values for several

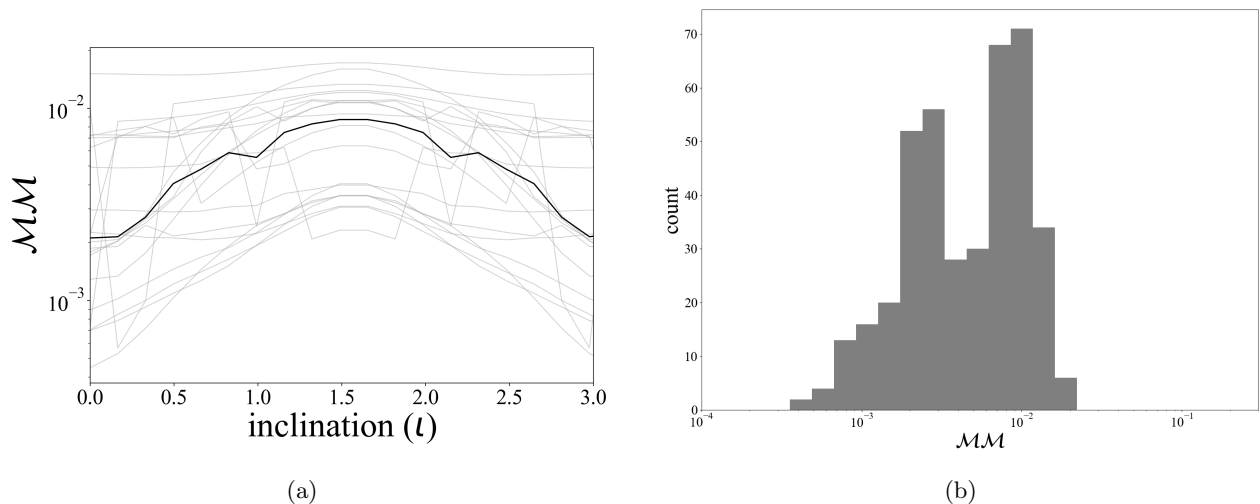


FIG. 7: Mismatches between eccentric, non-precessing MAYA waveforms and TEOBResumS-DALI waveforms using a flat noise curve over 20 different values of inclination. a) Mismatches as a function of inclination. The black line is the median for all systems. The faint lines show all of the individual systems. b) Distribution of mismatches.

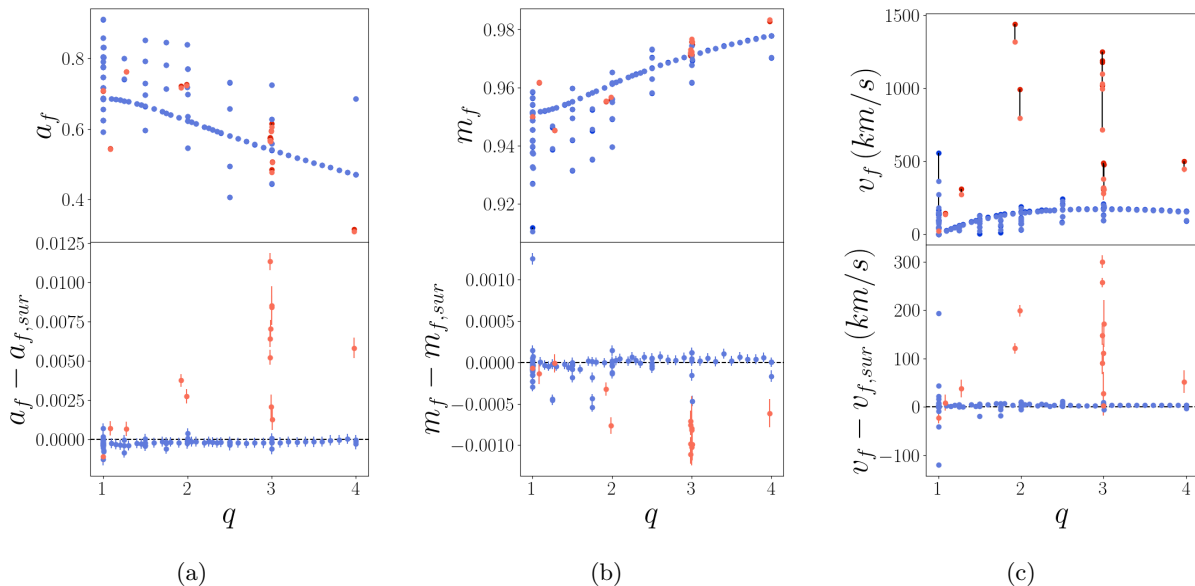


FIG. 8: Comparison of the properties of the remnant black hole computed from the NR simulation and predicted by NRSur7dq4Remnant. The top panels show the remnant property as a function of mass ratio. Non-precessing systems appear in blue and precessing systems appear in orange. The darker points show the NR values and the lighter points show the model predictions. The points referring to the same systems are connected by black lines. The bottom panel shows the residuals resulting from subtracting the model predicted value from the NR value. The vertical lines are the uncertainty in the model predictions.

modes as a function of mass ratio. While there does not appear to be a strong correlation between the impact of COM corrections and mass ratio, the figure does reveal that certain modes are more impacted than others. In particular, the $\ell = 4$, $m = 2$ mode has mismatches up to $\sim 10^{-2}$.

Using the `mayawaves` library, our waveforms can be read in their raw form or with COM corrections. The

waveforms stored in the PYCBC compatible format [76–78] have been corrected for COM drift.

VII. CONCLUSION

This paper introduces the second MAYA catalog of NR waveforms. It contains 181 waveforms that fill in and ex-

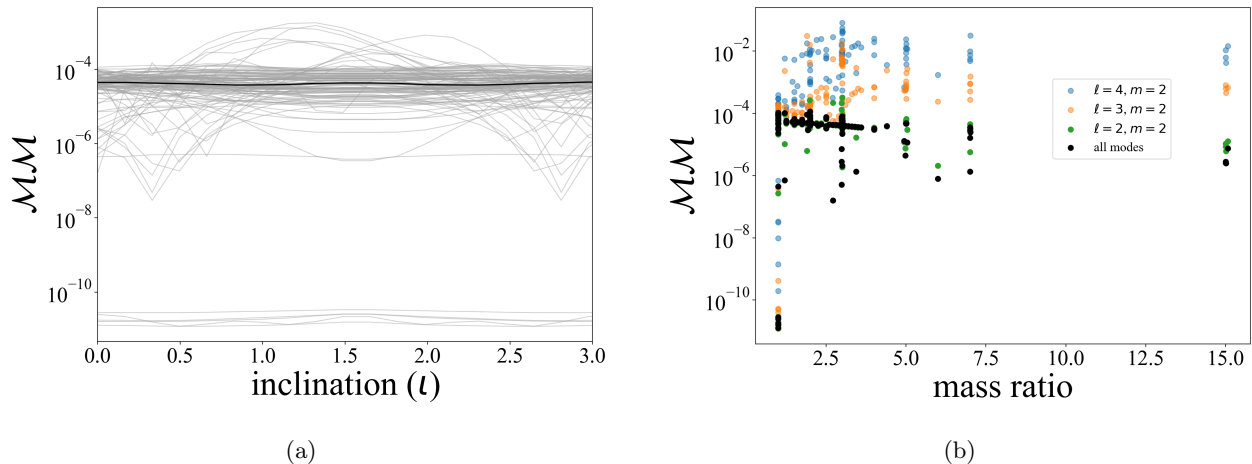


FIG. 9: Mismatches between COM drift corrected waveforms and raw waveforms. a) The mismatch including all modes vs inclination. Each system is represented by a light gray line with the darker line showing the median value. b) The mismatch for various modes and for all modes (at face-on orientation) as a function of mass ratio.

pand our coverage of the BBH parameter space. This includes 80 from an eccentric suite ranging up to eccentricities of 0.1, as well as 7 systems with both precession and eccentricity. It also includes 38 waveforms studying secondary spin, 9 simulations as NR followup for LVK events, and 31 simulations placed to optimize parameter space coverage.

As the most accurate way of studying the merger of comparably massed objects, NR waveforms are crucial for understanding the observations of current and next-generation GW detectors. We must, therefore, ensure we have sufficient NR coverage of the anticipated parameter space. This catalog makes significant strides towards this goal by pushing and filling in considerable gaps in existing NR coverage of the BBH parameter space. With mass ratios up to $q = 15$, highly precessing simulations, and an extensive eccentric suite, this catalog greatly improves the coverage of public NR catalogs.

By performing a thorough error analysis and comparison to other NR codes, we are confident in the accuracy and reliability of the waveforms presented in this catalog.

Through a comparison to state-of-the-art GW models, we show consistency but also highlight the continuing need for NR waveforms particularly in the less well understood precessing space.

The waveforms are provided at <https://cgp.ph.utexas.edu/waveform> and can be read using the `mayawaves` python package. We have also updated the previous Georgia Tech catalog to include more data by using the new format, leading to a total of 635 public waveforms. All waveforms that fit the requirements are also provided in the format described in [76] for use with PYCBC.

Acknowledgements The catalog and analysis presented in this paper are possible due to grants NASA 80NSSC21K0900, NSF 2207780 and NSF 2114582. The computing resources necessary to perform the simulations in this catalog were provided by XSEDE PHY120016, TACC PHY20039, TACC NR-Catalog and TACC Template-Placement. This work was done by members of the Weinberg Institute and has an identifier of UTWI-32-2023.

-
- [1] LIGO Scientific Collaboration, Virgo Collaboration, and KAGRA Collaboration (LIGO Scientific, VIRGO, KAGRA), (2021), arXiv:2111.03606 [gr-qc].
 - [2] R. Abbott et al. (LIGO Scientific, VIRGO), (2021), arXiv:2108.01045 [gr-qc].
 - [3] R. Abbott et al. (LIGO Scientific, Virgo), Phys. Rev. X **11**, 021053 (2021), arXiv:2010.14527 [gr-qc].
 - [4] B. P. Abbott et al. (LIGO Scientific, Virgo), Phys. Rev. X **9**, 031040 (2019), arXiv:1811.12907 [astro-ph.HE].
 - [5] LIGO Scientific Collaboration and Virgo Collaboration (LIGO Scientific, Virgo), Astrophys. J. Lett. **896**, L44 (2020), arXiv:2006.12611 [astro-ph.HE].
 - [6] V. Gayathri, J. Healy, J. Lange, B. O’Brien, M. Szczepanczyk, I. Bartos, M. Campanelli, S. Klimentko, C. O. Lousto, and R. O’Shaughnessy, Nature Astron. **6**, 344 (2022), arXiv:2009.05461 [astro-ph.HE].
 - [7] I. M. Romero-Shaw, P. D. Lasky, and E. Thrane, Astrophys. J. Lett. **921**, L31 (2021), arXiv:2108.01284 [astro-ph.HE].
 - [8] J. Baker et al., arXiv e-prints, arXiv:1907.06482 (2019), arXiv:1907.06482 [astro-ph.IM].
 - [9] P. Amaro-Seoane et al., arXiv e-prints, arXiv:1702.00786 (2017), arXiv:1702.00786 [astro-ph.IM].

- [10] T. Robson, N. J. Cornish, and C. Liu, *Classical and Quantum Gravity* **36**, 105011 (2019).
- [11] M. Punturo *et al.*, *Class. Quant. Grav.* **27**, 194002 (2010).
- [12] M. Abernathy *et al.*, EGO (2011).
- [13] M. Evans *et al.*, arXiv e-prints, arXiv:2109.09882 (2021), arXiv:2109.09882 [astro-ph.IM].
- [14] LIGO Scientific Collaboration and Virgo Collaboration (LIGO Scientific, Virgo), *Astrophys. J. Lett.* **913**, L7 (2021), arXiv:2010.14533 [astro-ph.HE].
- [15] LIGO Scientific Collaboration, Virgo Collaboration, and KAGRA Collaboration (LIGO Scientific, VIRGO, KAGRA), (2021), arXiv:2112.06861 [gr-qc].
- [16] S. Isoyama, R. Sturani, and H. Nakano, (2020), 10.1007/978-981-15-4702-7_31-1, arXiv:2012.01350 [gr-qc].
- [17] L. Blanchet, *Living Rev. Rel.* **17**, 2 (2014), arXiv:1310.1528 [gr-qc].
- [18] G. Schäfer and P. Jaranowski, *Living Rev. Rel.* **21**, 7 (2018), arXiv:1805.07240 [gr-qc].
- [19] T. Futamase and Y. Itoh, *Living Rev. Rel.* **10**, 2 (2007).
- [20] L. Blanchet, G. Faye, B. R. Iyer, and S. Sinha, *Class. Quant. Grav.* **25**, 165003 (2008), [Erratum: *Class. Quant. Grav.* **29**, 239501 (2012)], arXiv:0802.1249 [gr-qc].
- [21] G. Faye, S. Marsat, L. Blanchet, and B. R. Iyer, *Class. Quant. Grav.* **29**, 175004 (2012), arXiv:1204.1043 [gr-qc].
- [22] G. Faye, L. Blanchet, and B. R. Iyer, *Class. Quant. Grav.* **32**, 045016 (2015), arXiv:1409.3546 [gr-qc].
- [23] T. Hinderer and E. E. Flanagan, *Phys. Rev. D* **78**, 064028 (2008), arXiv:0805.3337 [gr-qc].
- [24] J. Miller and A. Pound, *Phys. Rev. D* **103**, 064048 (2021), arXiv:2006.11263 [gr-qc].
- [25] L. Barack and A. Pound, *Rept. Prog. Phys.* **82**, 016904 (2019), arXiv:1805.10385 [gr-qc].
- [26] M. van de Meent and H. P. Pfeiffer, *Phys. Rev. Lett.* **125**, 181101 (2020), arXiv:2006.12036 [gr-qc].
- [27] B. Wardell, A. Pound, N. Warburton, J. Miller, L. Durkan, and A. Le Tiec, (2021), arXiv:2112.12265 [gr-qc].
- [28] N. Warburton, A. Pound, B. Wardell, J. Miller, and L. Durkan, *Phys. Rev. Lett.* **127**, 151102 (2021), arXiv:2107.01298 [gr-qc].
- [29] A. Albertini, A. Nagar, A. Pound, N. Warburton, B. Wardell, L. Durkan, and J. Miller, *Phys. Rev. D* **106**, 084061 (2022), arXiv:2208.01049 [gr-qc].
- [30] A. Albertini, A. Nagar, A. Pound, N. Warburton, B. Wardell, L. Durkan, and J. Miller, *Phys. Rev. D* **106**, 084062 (2022), arXiv:2208.02055 [gr-qc].
- [31] T. W. Baumgarte and S. L. Shapiro, *Phys. Rev. D* **59**, 024007 (1998), arXiv:gr-qc/9810065.
- [32] T. W. Baumgarte and S. L. Shapiro, *Numerical Relativity: Solving Einstein's Equations on the Computer* (Cambridge University Press, 2010).
- [33] T. W. Baumgarte and S. L. Shapiro, *Phys. Rev. D* **59**, 024007 (1998).
- [34] J. Lange *et al.*, *Phys. Rev. D* **96**, 104041 (2017), arXiv:1705.09833 [gr-qc].
- [35] B. P. Abbott *et al.* (LIGO Scientific, Virgo), *Phys. Rev. D* **94**, 064035 (2016), arXiv:1606.01262 [gr-qc].
- [36] J. Calderon Bustillo, N. Sanchis-Gual, S. H. W. Leong, K. Chandra, A. Torres-Forne, J. A. Font, C. Herdeiro, E. Radu, I. C. F. Wong, and T. G. F. Li, (2022), arXiv:2206.02551 [gr-qc].
- [37] V. Varma, S. E. Field, M. A. Scheel, J. Blackman, D. Gerosa, L. C. Stein, L. E. Kidder, and H. P. Pfeiffer, *Phys. Rev. Research.* **1**, 033015 (2019), arXiv:1905.09300 [gr-qc].
- [38] A. Bohé *et al.*, *Phys. Rev. D* **95**, 044028 (2017), arXiv:1611.03703 [gr-qc].
- [39] S. Khan, S. Husa, M. Hannam, F. Ohme, M. Pürrer, X. Jiménez Forteza, and A. Bohé, *Phys. Rev. D* **93**, 044007 (2016), arXiv:1508.07253 [gr-qc].
- [40] J. Blackman, S. E. Field, M. A. Scheel, C. R. Galle, C. D. Ott, M. Boyle, L. E. Kidder, H. P. Pfeiffer, and B. Szilágyi, *Phys. Rev. D* **96**, 024058 (2017), arXiv:1705.07089 [gr-qc].
- [41] S. Husa, S. Khan, M. Hannam, M. Pürrer, F. Ohme, X. Jiménez Forteza, and A. Bohé, *Phys. Rev. D* **93**, 044006 (2016), arXiv:1508.07250 [gr-qc].
- [42] A. Taracchini *et al.*, *Phys. Rev. D* **89**, 061502 (2014), arXiv:1311.2544 [gr-qc].
- [43] M. Hannam, P. Schmidt, A. Bohé, L. Haegel, S. Husa, F. Ohme, G. Pratten, and M. Pürrer, *Phys. Rev. Lett.* **113**, 151101 (2014), arXiv:1308.3271 [gr-qc].
- [44] L. Santamaria *et al.*, *Phys. Rev. D* **82**, 064016 (2010), arXiv:1005.3306 [gr-qc].
- [45] H. Nakano, Y. Zlochower, C. O. Lousto, and M. Campanelli, *Phys. Rev. D* **84**, 124006 (2011), arXiv:1108.4421 [gr-qc].
- [46] G. Pratten *et al.*, *Phys. Rev. D* **103**, 104056 (2021), arXiv:2004.06503 [gr-qc].
- [47] D. Ferguson, K. Jani, P. Laguna, and D. Shoemaker, *Phys. Rev. D* **104**, 044037 (2021), arXiv:2006.04272 [gr-qc].
- [48] M. Pürrer and C.-J. Haster, *Phys. Rev. Res.* **2**, 023151 (2020), arXiv:1912.10055 [gr-qc].
- [49] A. H. Mroué *et al.*, *Physical Review Letters* **111**, 241104 (2013), arXiv:1304.6077 [gr-qc].
- [50] M. Boyle *et al.*, *Classical and Quantum Gravity* **36**, 195006 (2019), arXiv:1904.04831 [gr-qc].
- [51] N. Deppe, W. Throwe, L. E. Kidder, N. L. Fischer, F. Hébert, J. Moxon, C. Armaza, G. S. Bonilla, P. Kumar, G. Lovelace, E. O'Shea, H. P. Pfeiffer, M. A. Scheel, S. A. Teukolsky, I. Anantpurkar, M. Boyle, F. Foucart, M. Giesler, J. S. Guo, D. A. B. Izzo, Y. Kim, I. Legred, D. Li, A. Macedo, D. Melchor, M. Morales, K. C. Nelli, T. Ramirez, H. R. Ritter, J. Sanchez, S. Thomas, N. A. Wittek, and T. Wlodarczyk, "Spectre," (2021).
- [52] F. Löffler *et al.*, *Class. Quant. Grav.* **29**, 115001 (2012), arXiv:1111.3344 [gr-qc].
- [53] K. Jani, J. Healy, J. A. Clark, L. London, P. Laguna, and D. Shoemaker, *Class. Quant. Grav.* **33**, 204001 (2016), arXiv:1605.03204 [gr-qc].
- [54] J. Healy, C. O. Lousto, Y. Zlochower, and M. Campanelli, *Class. Quant. Grav.* **34**, 224001 (2017), arXiv:1703.03423 [gr-qc].
- [55] J. Healy, C. O. Lousto, J. Lange, R. O'Shaughnessy, Y. Zlochower, and M. Campanelli, *Phys. Rev. D* **100**, 024021 (2019), arXiv:1901.02553 [gr-qc].
- [56] J. Healy and C. O. Lousto, *Phys. Rev. D* **105**, 124010 (2022), arXiv:2202.00018 [gr-qc].
- [57] J. Healy and C. O. Lousto, *Phys. Rev. D* **102**, 104018 (2020).
- [58] K. Jani, D. Shoemaker, and C. Cutler, *Nature Astron.* **4**, 260 (2019), arXiv:1908.04985 [gr-qc].

- [59] K. Chandra, V. Gayathri, J. C. Bustillo, and A. Pai, *Phys. Rev. D* **102**, 044035 (2020).
- [60] R. Abbott et al. (LIGO Scientific, VIRGO, KAGRA), *Astron. Astrophys.* **659**, A84 (2022), arXiv:2105.15120 [astro-ph.HE].
- [61] J. Calderón Bustillo, C. Evans, J. A. Clark, G. Kim, P. Laguna, and D. Shoemaker, (2019), 10.1038/s42005-020-00446-7, arXiv:1906.01153 [gr-qc].
- [62] D. Ferguson, S. Ghonge, J. A. Clark, J. Calderon Bustillo, P. Laguna, D. Shoemaker, and J. Calderon Bustillo, *Phys. Rev. Lett.* **123**, 151101 (2019), arXiv:1905.03756 [gr-qc].
- [63] J. Healy, P. Laguna, and D. Shoemaker, *Class. Quant. Grav.* **31**, 212001 (2014), arXiv:1407.5989 [gr-qc].
- [64] J. Calderón Bustillo, J. A. Clark, P. Laguna, and D. Shoemaker, *Phys. Rev. Lett.* **121**, 191102 (2018).
- [65] J. Calderón Bustillo, S. H. W. Leong, and K. Chandra, (2022), arXiv:2211.03465 [gr-qc].
- [66] D. Ferguson et al., (2023), arXiv:2309.00653 [astro-ph.IM].
- [67] D. Ferguson, S. Anne, M. Gracia-Linares, H. Iglesias, A. Jan, E. Martinez, L. Lu, F. Meoni, R. Nowicki, M. Trostel, B.-J. Tsao, and F. Valorz, “mayawaves,” (2023).
- [68] E. Schnetter, S. H. Hawley, and I. Hawke, *Class. Quant. Grav.* **21**, 1465 (2004), arXiv:gr-qc/0310042 [gr-qc].
- [69] M. Ansorg, B. Bruegmann, and W. Tichy, *Phys. Rev. D* **70**, 064011 (2004), arXiv:gr-qc/0404056.
- [70] J. M. Bowen and J. W. York, *Phys. Rev. D* **21**, 2047 (1980).
- [71] J. Healy, C. O. Lousto, H. Nakano, and Y. Zlochower, *Class. Quant. Grav.* **34**, 145011 (2017), arXiv:1702.00872 [gr-qc].
- [72] M. Campanelli, C. O. Lousto, P. Marronetti, and Y. Zlochower, *Phys. Rev. Lett.* **96**, 111101 (2006).
- [73] J. G. Baker, J. Centrella, D.-I. Choi, M. Koppitz, and J. van Meter, *Phys. Rev. Lett.* **96**, 111102 (2006), gr-qc/0511103.
- [74] S. Husa, I. Hinder, and C. Lechner, *Computer Physics Communications* **174**, 983 (2006), gr-qc/0404023.
- [75] C. O. Lousto, H. Nakano, Y. Zlochower, and M. Campanelli, *Phys. Rev. D* **82**, 104057 (2010), arXiv:1008.4360 [gr-qc].
- [76] P. Schmidt, I. W. Harry, and H. P. Pfeiffer, (2017), arXiv:1703.01076 [gr-qc].
- [77] LIGO Scientific Collaboration, “LIGO Algorithm Library - LALSuite,” free software (GPL) (2018).
- [78] A. Nitz, I. Harry, D. Brown, C. M. Biwer, J. Willis, T. D. Canton, C. Capano, L. Pekowsky, T. Dent, A. R. Williamson, S. De, G. Davies, M. Cabero, D. Macleod, B. Machenschalk, S. Reyes, P. Kumar, T. Massinger, F. Pannarale, dfinstad, M. Tápai, S. Fairhurst, S. Khan, L. Singer, S. Kumar, A. Nielsen, shasvath, idorring-ton92, A. Lenon, and H. Gabbard, “gwastro/pycbc: Pycbc release v1.15.4,” (2020).
- [79] D. Ferguson, (2022), arXiv:2209.15144 [gr-qc].
- [80] P. C. Peters, *Phys. Rev.* **136**, B1224 (1964).
- [81] J. Samsing, *Phys. Rev. D* **97**, 103014 (2018).
- [82] C. L. Rodriguez, P. Amaro-Seoane, S. Chatterjee, and F. A. Rasio, *Phys. Rev. Lett.* **120**, 151101 (2018).
- [83] M. Morscher, B. Pattabiraman, C. Rodriguez, F. A. Rasio, and S. Umbreit, *The Astrophysical Journal* **800**, 9 (2015).
- [84] M. Zevin, J. Samsing, C. Rodriguez, C.-J. Haster, and E. Ramirez-Ruiz, *The Astrophysical Journal* **871**, 91 (2019).
- [85] A. Ramos-Buades, S. Husa, and G. Pratten, *Phys. Rev. D* **99**, 023003 (2019), arXiv:1810.00036 [gr-qc].
- [86] R. Abbott et al. (LIGO Scientific, Virgo), *Phys. Rev. Lett.* **125**, 101102 (2020), arXiv:2009.01075 [gr-qc].
- [87] R. Gamba, M. Breschi, G. Carullo, S. Albanesi, P. Rettegno, S. Bernuzzi, and A. Nagar, *Nature Astron.* **7**, 11 (2023), arXiv:2106.05575 [gr-qc].
- [88] J. Calderón Bustillo, N. Sanchis-Gual, A. Torres-Forné, J. A. Font, A. Vajpeyi, R. Smith, C. Herdeiro, E. Radu, and S. H. W. Leong, *Phys. Rev. Lett.* **126**, 081101 (2021), arXiv:2009.05376 [gr-qc].
- [89] P. Ajith et al., *Classical and Quantum Gravity* **29**, 124001 (2012), arXiv:1201.5319 [gr-qc].
- [90] I. Hinder et al., *Classical and Quantum Gravity* **31**, 025012 (2013), arXiv:1307.5307 [gr-qc].
- [91] J. Healy et al., *Phys. Rev. D* **97**, 064027 (2018), arXiv:1712.05836 [gr-qc].
- [92] D. Chiaramello and A. Nagar, *Phys. Rev. D* **101**, 101501 (2020), arXiv:2001.11736 [gr-qc].
- [93] A. Nagar, A. Bonino, and P. Rettegno, *Phys. Rev. D* **103**, 104021 (2021), arXiv:2101.08624 [gr-qc].
- [94] A. Nagar and P. Rettegno, *Phys. Rev. D* **104**, 104004 (2021), arXiv:2108.02043 [gr-qc].
- [95] A. Placidi, S. Albanesi, A. Nagar, M. Orselli, S. Bernuzzi, and G. Grignani, *Phys. Rev. D* **105**, 104030 (2022), arXiv:2112.05448 [gr-qc].
- [96] V. Varma, D. Gerosa, L. C. Stein, F. Hébert, and H. Zhang, *Phys. Rev. Lett.* **122**, 011101 (2019), arXiv:1809.09125 [gr-qc].
- [97] V. Varma, L. C. Stein, and D. Gerosa, “vijayvarma392/surfinBH: Surrogate Final BH properties,” (2018).
- [98] M. Boyle, D. Iozzo, and L. C. Stein, “moble/scri: v1.2,” (2020).
- [99] M. Boyle, *Phys. Rev. D* **87**, 104006 (2013).
- [100] M. Boyle, L. E. Kidder, S. Ossokine, and H. P. Pfeiffer, “Gravitational-wave modes from precessing black-hole binaries,” (2014), arXiv:1409.4431 [gr-qc].
- [101] M. Boyle, *Phys. Rev. D* **93**, 084031 (2016).
- [102] C. J. Woodford, M. Boyle, and H. P. Pfeiffer, *Phys. Rev. D* **100**, 124010 (2019), arXiv:1904.04842 [gr-qc].